Bone Marrow Dosimetry Using ^{124}I-PET

Jazmin Schwartz[1], John L. Humm[1], Chaitanya R. Divgi[2], Steven M. Larson[3], and Joseph A. O'Donoghue[1]

[1]Department of Medical Physics, Memorial Sloan-Kettering Cancer Center, New York, New York; [2]Department of Radiology, Columbia University, Columbia University Medical Center, New York, New York; and [3]Department of Radiology, Nuclear Medicine Service, Memorial Sloan-Kettering Cancer Center, New York, New York

Bone marrow is usually dose-limiting for radioimmunotherapy. In this study, we directly estimated red marrow activity concentration and the self-dose component of absorbed radiation dose to red marrow based on PET/CT of 2 different ^{124}I-labeled antibodies (cG250 and huA33) and compared the results with plasma activity concentration and plasma-based dose estimates. **Methods:** Two groups of patients injected with ^{124}I-labeled monoclonal antibodies (11 patients with renal cancer receiving ^{124}I-cG250 and 5 patients with colorectal cancer receiving ^{124}I-huA33) were imaged by PET or PET/CT on 2 or 3 occasions after infusion. Regions of interest were drawn over several lumbar vertebrae, and red marrow activity concentration was quantified. Plasma activity concentration was also quantified using multiple patient blood samples. The red marrow–to–plasma activity concentration ratio (RMPR) was calculated at the times of imaging. The self-dose component of the absorbed radiation dose to the red marrow was estimated from the images, from the plasma measurements, and using a combination of both sets of measurements. **Results:** RMPR was observed to increase with time for both groups of patients. Mean ($\pm$SD) time-dependent RMPR (RMPR(t)) for the cG250 group increased from 0.13 ± 0.06 immediately after infusion to 0.23 ± 0.09 at approximately 6 d after infusion. For the huA33 group, mean RMPR(t) was 0.10 ± 0.04 immediately after infusion, 0.13 ± 0.05 approximately 2 d after infusion, and 0.20 ± 0.09 approximately 7 d after infusion. Plasma-based estimates of red marrow self-dose tended to be greater than image-based values by, on average, 11% and 47% for cG250 and huA33, respectively, but by as much as -73% to 62% for individual patients. The hybrid method combining RMPR(t) and plasma activity concentration provided a closer match to the image-based dose estimates (average discrepancies, -2% and 18% for cG250 and huA33, respectively). **Conclusion:** These results suggest that the assumption of time-independent proportionality between red marrow and plasma activity concentration may be too simplistic. Individualized imaged-based dosimetry is probably required for the optimal therapeutic delivery of radiolabeled antibodies, which does not compromise red marrow and may allow, for some patients, a substantial increase in administered activity and thus tumor dose.

Key Words: dosimetry; marrow; PET

The goal in radioimmunotherapy is to maximize the absorbed dose to target volumes while ensuring that delivery to vulnerable normal organs is within acceptable limits. Typically, for radioimmunotherapy the dose-limiting organ is the red marrow (i.e., the blood-forming cells of the bone marrow).

Several methods have been developed for red marrow dosimetry and can generally be divided into image- and blood sample–based approaches. The most commonly used quantitative imaging technique for dosimetry is the conjugate-view method. Anterior and posterior images are acquired with a γ-camera at multiple time points after administration of the radiolabeled antibody. Geometric mean counts are obtained for regions of interest (ROIs) placed over targets of interest. These may then be corrected for attenuation and scatter and converted to activities or activity concentrations (1,2). The resulting time–activity data are used to determine the pharmacokinetics of the antibody in the organs of interest, and the area under the time–activity curve is used as the basis for calculation of radiation dose to tissues, including red marrow.

Planar imaging has been used to quantify activity concentration for purposes of dosimetry, particularly for isotopes such as ^{131}I, which can be followed over many days. However, accuracy is limited by the approximate scatter and attenuation corrections generally used and the typically poor target-tissue visualization and delineation on planar images (3). Methods to obtain quantitative SPECT images have and continue to be developed (4), but to our knowledge, their application to bone marrow dosimetry has not been reported.

In an alternative approach, blood or plasma activity concentration may be used as a surrogate (with a scaling factor) of the activity concentration in red marrow for agents that do not specifically bind to marrow cellular components or otherwise specifically localize in marrow (5–8). Measurements of blood or plasma activity concentration at multiple times after administration may be used as a basis for red marrow absorbed dose estimation (7). The blood-based method assumes that extracellular fluid in the marrow spaces has the same activity concentration as plasma and, consequently, that the activity concentration ratio of red marrow to plasma is a constant, equal to the fraction of red marrow composed of extracellular fluid (7). Alternatively, the ratio may be expressed with respect to whole blood (8) (i.e., a red marrow–to–blood

ratio), for which a value of 0.32–0.36 is typically used (*9*). Evaluation of this approach was performed in a 7-institution trial in which marrow dose was estimated by a centralized facility using standardized methods and compared with estimates provided by the individual participants. The study showed that independent use of the blood method resulted in red marrow dose estimates with mean and maximum differences of 8% and 30%, respectively (*10*). However, red marrow absorbed dose as calculated by this approach has not proven to be a good predictor of hematologic toxicity, particularly for nuclides other than [131]I (*11,12*).

PET, like γ-camera–based SPECT, can provide quantitative, 3-dimensional images that may be used to study biochemical and physiologic processes in the human body (*13,14*). However, PET has several physical advantages, including a more accurate attenuation correction that enables calibration of the scanner in terms of the absolute activity concentration in a tissue (i.e., Bq/mL). This advantage is of fundamental importance in accurately determining radiation doses to tissues or organs. In addition, PET provides higher sensitivity and spatial resolution than SPECT or planar γ-camera imaging.

The most commonly used PET radionuclide, ^{18}F, has a half-life too short (110 min) to encompass the long retention and slow biokinetic behavior of large molecules such as antibodies. Among the currently available positron emitters, [124]I has the longest physical half-life (4.2 d) and PET/CT using [124]I-labeled antibodies has been used to successfully image antibody biodistribution over timescales of a week or more after administration (*15,16*). However, [124]I poses several challenges to quantitative PET. The most important of these factors are its low (0.24) positron yield and emission of prompt γ-rays (in coincidence with the positron decay) that have energies within the annihilation energy window (350–650 keV). Despite these difficulties, [124]I-PET has been shown to be accurate to within 10% for images acquired in 2-dimensional mode (*17–19*).

In the current study, PET and PET/CT images of patients who had been administered [124]I-radiolabeled antibodies were used to investigate the relationship between red marrow and plasma activity concentrations as a function of time after injection. The impact of this relationship on estimated absorbed dose to red marrow was assessed and compared with the conventional plasma-based method. To our knowledge, this is the first time that PET has been used for bone marrow dosimetry.

MATERIALS AND METHODS

Data from 2 groups of patients who were administered [124]I-labeled antibodies intravenously were included in this analysis: 11 patients with renal cell carcinoma administered [124]I-labeled cG250 (group 1), and 5 patients with colorectal cancer administered [124]I-labeled huA33 (group 2). Patients in group 1 were injected intravenously with 185 MBq/10 mg (5 mCi/10 mg) of [124]I-cG250 in 50 mL of 5% human serum albumin over 20 min. Patients in group 2 were injected intravenously with 148–370 MBq/10 mg (4–10 mCi/10 mg) of [124]I-huA33 in 5–30 mL of 5% human serum albumin over 5 min. For both groups,

the respective clinical studies were designed to facilitate comparisons between [124]I-immunoPET imaging performed immediately before surgery and analysis of surgically removed tissues. The results of these comparisons have been reported elsewhere (*15,16,20,21*). However, for current purposes it may be noted that patient selection criteria for both groups specified normal hematologic parameters and no evidence of metastatic bone disease. Neither cG250 nor huA33 antibody binds specifically to hematopoietic cells.

All patients underwent [124]I-PET on at least 2 occasions. Partial-body (xiphoid to pelvis) scans were acquired on an Advance PET, Discovery LS PET/CT, or Discovery STE PET/CT scanner (GE Healthcare). Images typically consisted of 2–3 fields of view with total durations of 20–40 min. Attenuation correction was performed using [68]Ge transmission scans (Advance) or low-dose (80 mA, 140 kVp) CT scans (Discovery). Patients in group 1 ([124]I-cG250) were imaged on the Advance within 3 h of administration (PET 1A) and then on the GE Discovery LS or STE (PET 1B) approximately 1 wk later. Patients in group 2 ([124]I-huA33) were imaged on the Discovery STE on 3 occasions: within 3 h (PET 2A), at 2–3 d (PET 2B), and at 3–8 d (PET 2C) after administration. All CT scans were acquired without contrast material. Blood samples were drawn at multiple times immediately after injection and subsequently at the times of image acquisition. Blood samples were collected in heparinized vials and centrifuged. Thereafter, the activity concentrations in blood plasma were measured using a Wizard well scintillation counter (Wallac) together with appropriate [124]I standards.

Image Registration and ROIs

Image sets were coregistered using CT or [68]Ge transmission scans using software developed in-house (*22*). Particular emphasis was placed on image matching in the L1–L5 region. The derived transformation matrices were used to align the PET image data. For marrow activity quantification, ROIs were drawn on lumbar vertebral bodies as visualized by the CT component of the terminal PET/CT scan (PET 1B and PET 2C). ROIs were drawn on all CT slices where lumbar vertebrae were present (typically 5–8 slices per vertebra). On each CT slice, 2 sets of ROIs were drawn: an exterior ROI encompassing the entire vertebral body—used to derive a correction factor for the partial-volume effect; and a smaller interior one encompassing the trabecular core of the vertebral body—used for activity concentration estimation. The ROIs were subsequently transferred to all other images using the transformation matrices derived from image registration. Figure 1 shows the placement of 2 ROIs on a representative slice from a patient in the study.

Corrections for Partial-Volume Averaging and Trabecular Bone

Figure 1 summarizes the analysis steps and corrections described below. The volumes of each vertebral body were estimated on the basis of summed areas of the exterior ROI, and an equivalent spheric diameter (D_e) was calculated according to $D_e = \sqrt[3]{6V/\pi}$. Recovery coefficients were then determined by interpolation from previously measured look-up tables of recovery coefficients as a function of sphere diameter for the Advance, Discovery LS, and Discovery STE scanners as appropriate (*23*).

An additional correction factor for trabecular bone was incorporated on the basis of the following rationale: the interior vertebral ROI represents a mixture of trabecular bone and of marrow space contents (red and yellow marrow, blood vessels, extracellular matrix, and other components). In this study, for purposes of calculation, it
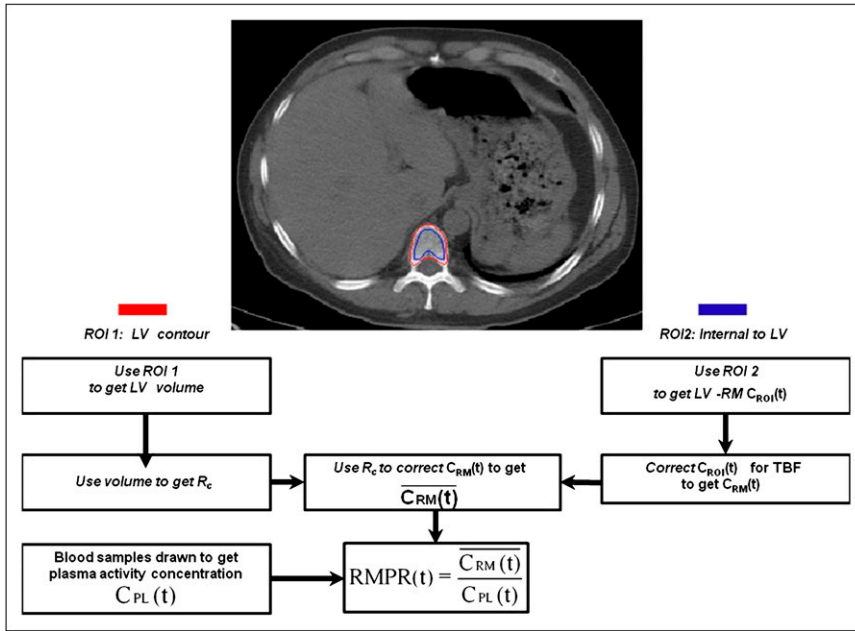
FIGURE 1. (Top) Representative slice showing positioning of each ROI. ROI 1 (red) is contour over LV for determining partial-volume effect correction; ROI 2 (blue) is internal to LV for determining average red marrow activity concentration. (Bottom) Flowchart of data analysis steps for calculation of RMPR(t). LV = lumbar vertebrae; Rc = recovery coefficient; $C_{ROI}(t)$ = activity concentration in ROI 2; TBF = trabecular bone fraction; $\overline{C_{RM}(t)}$ average activity concentration in LV.

was assumed that activity concentration within the marrow spaces is uniform and is equal to red marrow activity concentration. The potential errors associated with not taking account of an adipose component (i.e., yellow marrow) with reduced activity concentration are discussed later. It was also assumed that the activity concentration in trabecular bone is zero. This assumption is reasonable for radiolabeled antibodies such as cG250 and huA33 but would not hold for radiolabeled molecules that bind to bone components. Values of the fraction of the volume of the lumbar vertebrae composed of trabecular bone (f_{TB}) were taken to be 0.135 for male patients and 0.148 for female patients based on the work of Beddoe et al. (*24*), which is consistent with more recent studies (*25*). The multiplicative correction factor ($1/(1 - f_{TB})$) was then applied to the activity concentration estimates. In summary, for each vertebral body the red marrow activity concentration estimate, $C_{RM}(t)$, was derived from the ROI-based value, $C_{ROI}(t)$, according to

$$C_{RM}(t) = C_{ROI}(t)/(R_c(1 - f_{TB})),$$

where R_c is the recovery coefficient.

RMPR

We wished to examine the ratio of activity concentration in red marrow to that in blood plasma (red marrow–to–plasma activity concentration ratio, or RMPR) for these clinical data and compare this ratio with the time-independent value of 0.19 commonly used for radiation dosimetry purposes (*7*). For each clinical image, an average value, $\overline{C_{RM}}(t)$, was calculated over all vertebra-containing ROI slices,

$$\overline{C_{RM}}(t) = \frac{1}{n} \sum_{i=1}^{n} C_{RMi}(t),$$

where the sum is over the ith CT slice and n is the total number of slices included in the ROI. This value was used to evaluate the RMPR, viz

$$RMPR(t) = \frac{\overline{C_{RM}}(t)}{C_{PL}(t)},$$

where $C_{PL}(t)$ was the blood plasma activity concentration measured at the time of imaging.

Dosimetric Implications

To assess the potential impact of these findings for radiation dosimetry, self-doses to red marrow for time-dependent RMPR(t) were estimated and compared with the conventional case (i.e., a fixed RMPR value of 0.19).

Three separate scenarios were considered. In the first scenario, for the conventional case, RMPR was fixed and the red marrow activity concentration ($C_{RMp}(t)$) was represented by the plasma clearance curve, viz

$$C_{RMp}(t) = 0.19 \ C_{PL0} e^{-\lambda_{PL}t} e^{-\lambda_{phys}t},$$

where C_{PL0} and λ_{PL} are, respectively, the time-zero intercept and clearance rate of a monoexponential fit to the decay-corrected plasma data and λ_{phys} is the physical decay constant of ^{124}I (i.e., $\lambda_{phys} = 0.17 \ d^{-1}$). The cumulated activity concentration in red marrow, $\widetilde{C_{RMp}}$, is then given by

$$\widetilde{C_{RMp}} = \int_0^\infty C_{RMp}(t)dt = 0.19 \frac{C_{PL0}}{\lambda_{PL} + \lambda_{phys}}.$$

In the second scenario, a hybrid method in which the functional form of RMPR(t) was first determined by fitting a time-dependent exponential, $RMPR(t) = RMPR(0) \times e^{\lambda_{RMPR}t}$ and then convolving with the plasma function:

$$C_{RMtd}(t) = RMPR(0)C_{PL0}e^{\lambda_{RMPR}t} \ e^{-\lambda_{RM}t} \ e^{-\lambda_{phys}t}.$$

RMPR(0) and λ_{RMPR} are the fitting coefficients for RMPR(t). The cumulated activity concentration in red marrow, $\widetilde{C_{RMtd}}$, is then given by

$$\widetilde{C_{RMtd}} = \frac{RMPR(0)C_{PL0}}{\lambda_{RM} + \lambda_{phys} - \lambda_{RMPR}}.$$

In the third scenario, the average ROI activity concentration was used to directly calculate red marrow self-dose. Since this is

the most direct method for calculating dose, we used these values as the basis of comparison. Thus, the red marrow activity concentration was fit separately:

$$C_{RMI}(t) = C_{RMI0}e^{-\lambda_{RMI}t}e^{-\lambda_{phys}t}.$$

The cumulated activity concentration in red marrow, $\widetilde{C_{RMI}}$, is then given by

$$\widetilde{C_{RMI}} = \frac{C_{RMI0}}{\lambda_{RMI}+\lambda_{phys}}.$$

Once a cumulated activity concentration for red marrow is calculated, irrespective of method, the total residence time for red marrow, τ_{RM}, is given by

$$\tau_{RM} = \frac{\widetilde{C_{RM}}m_{RM}}{\rho_{RM}A_0},$$

where m_{RM} is total red marrow mass, ρ_{RM} is red marrow density (taken as 1 g/mL), and A_0 is the administered activity.

Finally, absorbed doses (in terms of mGy/MBq) were calculated using dose conversion factors (S factors) for red marrow self-dose:

$$D_{RM} = \tau_{RM}S_{RM \leftarrow RM}.$$

The values of red marrow mass and $S_{RM \leftarrow RM}$ for ^{124}I used in the calculations were taken from the OLINDA/EXM software application (26) for standard male and female phantoms as appropriate.

RESULTS

Individual patient plasma time–activity curves in terms of percentage of the injected dose per liter are shown in Figure 2 for patients injected with cG250 and huA33. Figures 2C and 2D shows the average red marrow activity concentration ($\overline{C_{RM}}$) for each patient. For the cG250 patients (Fig. 2C), $\overline{C_{RM}}$ ranged from 1.6% to 6.8%/L (average, 3.1% ± 1.7%/L) at the earlier imaging time and 0.19%–2.4%/L (average, 0.64% ± 0.6%/L) at the later one. For the huA33 patients (Fig. 2D), the corresponding values were 2.2%–3.8%/L (average, 2.9% ± 0.6%/L), 0.9%–2.2%/L (average, 1.4% ± 0.6%), and 0.08%–0.4%/L (average, 0.2% ± 0.1%/L) for the 3 imaging times, respectively.

The image-derived values of RMPR(t) for each patient are shown in Figure 3 for the cG250 and huA33 groups. RMPR(t) is not constant but is time-dependent and increases from the time of infusion. Moreover, it is not the same for all patients and can be considerably lower than 0.19 (dashed line in Fig. 3). The mean value (±SD) for RMPR(t) for the cG250 study group increased from 0.13 ± 0.06 at the time of the first image to 0.23 ± 0.09 at the time of the last image (~6 d after infusion). For the huA33 study group, the mean values of the RMPR(t) at the 3 imaging points were 0.10 ± 0.04 immediately after infusion, 0.13 ± 0.05 approximately 2 d after infusion, and 0.20 ± 0.09 approximately 7 d after infusion.

Figure 4 shows self-dose to red marrow for the calculation methods described previously. For ^{124}I-cG250 (Fig. 4A), the average dose per injected megabecquerel, calculated by integrating the PET ROI–derived activity concentration, $C_{RMI}(t)$, was 0.19 ± 0.09 mGy/MBq (range, 0.11–0.39; median, 0.14). The dose calculated using $C_{RMtd}(t)$ (i.e., the plasma activity concentration convolved with a time-dependent RMPR(t))
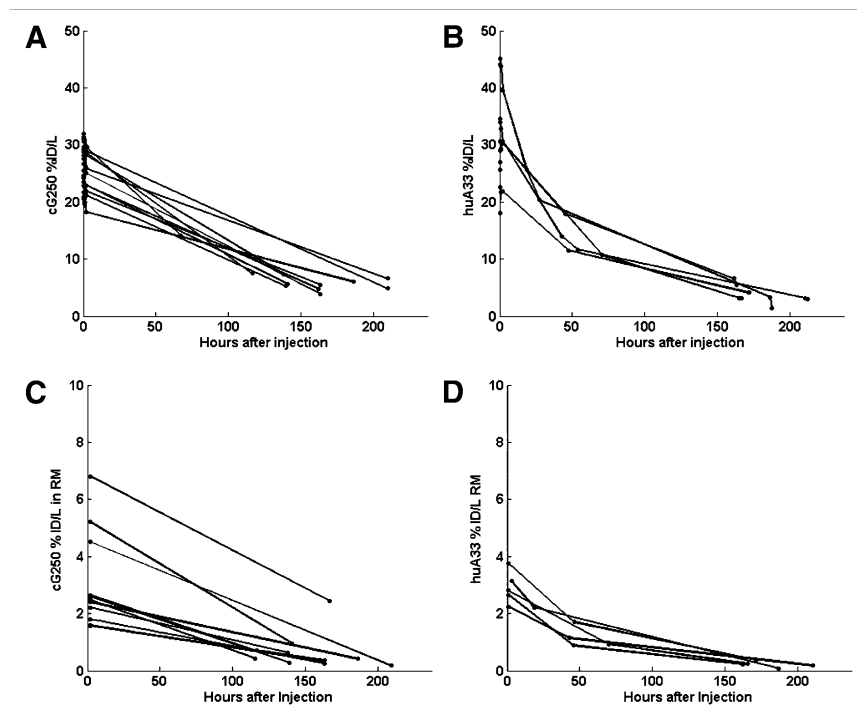

FIGURE 2. Percentage of injected dose (%ID) per liter of plasma for each patient antibody study group (cG250 [A] and huA33 [B]) as function of imaging time after infusion, and percentage injected activity present in red marrow in internal ROI for each patient (cG250 [C] and huA33 [D]) as function of imaging time after infusion. RM = red marrow.
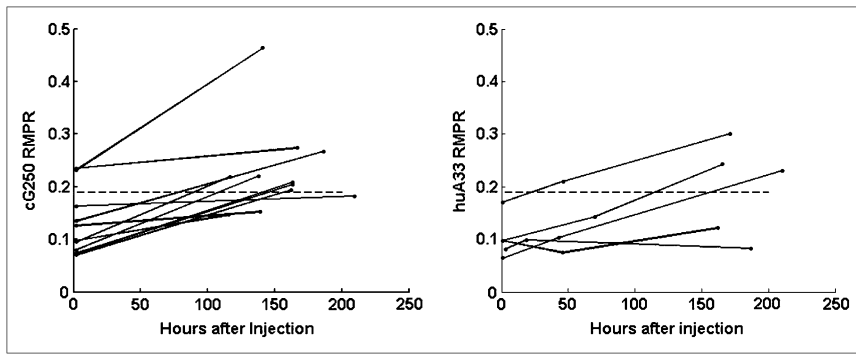
FIGURE 3. Image-derived time-dependent values of lumbar vertebrae RMPR(t) for each patient antibody study group (cG250 [A] and huA33 [B]) as function of imaging time after infusion. Dashed line represents conventional value of 0.19 (7).

was 0.19 ± 0.08 mGy/MBq (range, 0.11–0.35; median, 0.16) and that calculated using C_{RMP} (t) (i.e., the plasma activity concentration multiplied by a constant value of 0.19) was 0.20 ± 0.04 mGy/MBq (range, 0.17–0.29; median, 0.19). For individual patients, the self-dose calculated by the conventional plasma-based method was on average 11% ± 31% (median, 31%; range, −73% to 41%) greater than that calculated by the image-based method. The corresponding values comparing the image-based method with the hybrid image–

plasma convolution method were −2% ± 16% (median, −2%; range, −24% to 34%).

For ^{124}I-huA33 (Fig. 4B), the average self-doses per megabecquerel, calculated by integrating C_{RMI} (t), C_{RMtd} (t), or C_{RMP} (t), were 0.11 ± 0.02 mGy/MBq (range, 0.09–0.14; median, 0.10), 0.09 ± 0.04 mGy/MBq (range, 0.04–0.13; median, 0.09), and 0.20 ± 0.03 mGy/MBq (range, 0.16–0.23; median, 0.22), respectively. For individual patients, the conventional plasma-based method produced, on average, self-dose estimates 47% ± 17% (median, 57%; range, 20%–62%) greater than the image-based method. The corresponding comparison between the image-based and hybrid methods was 18% ± 30% (median, 7%; range, −13% to 59%).

DISCUSSION

In this study, red marrow self-dose was estimated by methods based on plasma activity concentration measurements or direct quantification of activity in the marrow spaces by ROI analysis of ^{124}I PET images. The derived estimates of RMPR suggests that this is not a constant but increases with time after radiolabeled antibody administration for patients injected with both ^{124}I-cG250 and ^{124}I-huA33.

Hinsdorf et al. (27) found that the red marrow–to–blood ratio in patients increased for up to 6 d after administration of ^{131}I-labeled anti-CD22 monoclonal antibody, where red marrow activity concentration was assessed by ROI analysis of sacral regions after scintigraphic imaging. In the same report Hinsdorf et al. also observed an increasing red marrow–to–blood ratio in tumor-bearing rats injected with ^{131}I-, ^{125}I-, ^{111}In-, and ^{188}Re-labeled BR96 monoclonal antibody, without specific uptake or evidence of tumor cells in marrow. An increasing red marrow–to–blood ratio is also consistent with the observations of Johnson et al. (6), who measured activity concentration in blood and bone marrow biopsies from patients at 2 times after infusion of ^{131}I-labeled Mc5 antibody.

In our study, the cG250 antigen (carbonic anhydrase 9) is largely absent from normal tissues with the exception of gastric mucosal cells and cells of the larger bile ducts (28). Similarly, immunohistochemical testing has shown huA33 to have limited normal-tissue reactivity, as antigen expression is restricted to colonic mucosal epithelia and lesions originating from there (29,30). Thus, specific binding to normal hematopoietic tissue is unlikely to be responsible
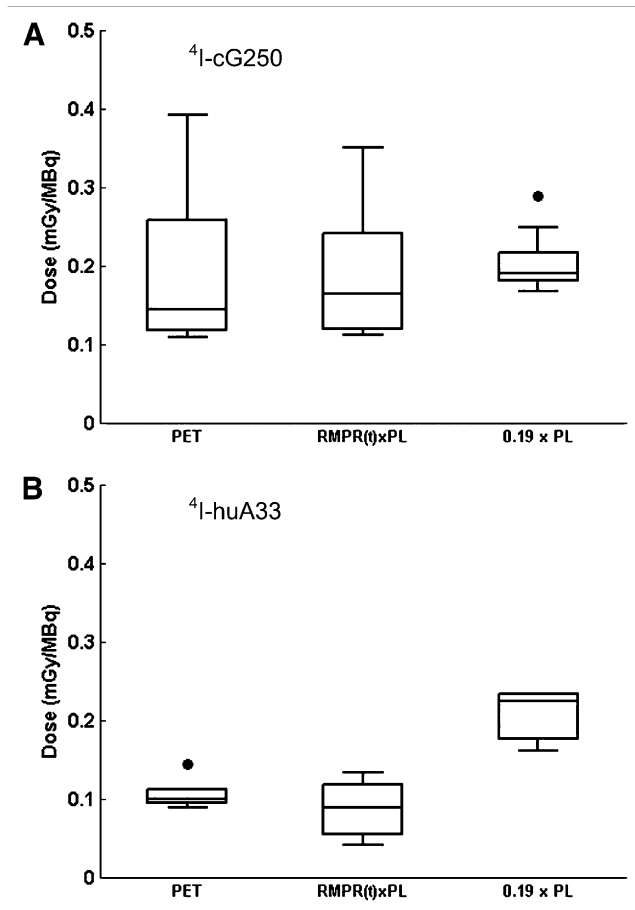

FIGURE 4. Box plot of calculated red marrow self-dose using 3 methods: directly from PET image, using RMPR(t) convolved with plasma (PL), and using conventional method with fixed RMPR of 0.19 for cG250 (A) and huA33 (B).

for our observations of increasing RMPR. It is also unlikely that subclinical metastatic activity in the marrow could be an explanation for the increasing RMPR, which was seen in the overwhelming majority of patients, whereas focal uptake, consistent with overt metastatic disease, was not seen in any. Hindorf et al. (27) speculated that that the slow apparent accumulation of antibodies may reflect binding to Fc receptor-expressing cells in the bone marrow.

The curves shown in Figure 3 for RMPR(t) indicate substantial intra- and intergroup variability. Although the use of a standard time-independent value of 0.19 for RMPR appears to be a reasonable compromise for the cG250 group, it is less so for the huA33 group (for which a smaller value would be more appropriate). However, at the level of individual patients, larger discrepancies between image-based and blood- or plasma-based dosimetry methods are seen. The existence of such discrepancies would be expected to impair attempts to derive meaningful dose–response relationships between hematologic toxicity and plasma-based dose estimates. It is also important to bear in mind that the comparisons discussed here apply only to the self-dose component of the overall red marrow dose and would be of most significance for radionuclides such as ^{177}Lu or ^{90}Y with little or no long-range photon emission. In contrast, for ^{131}I, which has a substantial cross-dose due to photon irradiation from activity elsewhere in the body, the effect would be diluted. Another factor that would have an impact is radionuclide half-life and kinetics in general. If most of the radiation dose to the red marrow were delivered within a short time of antibody administration, the conventional blood- or plasma-based dosimetry would be more likely to overestimate red marrow dose, compared with a situation in which the irradiation was protracted. In principle, this may be more severe for molecular vectors smaller than intact IgG with faster kinetics, such as Fab or F(ab′)$_2$ fragments. However, there are no analogous data on these smaller molecules, and if the slow accumulation of IgG reflects Fc binding, it may not occur for these types of antibody fragments.

The data presented in this paper indicate that plasma-based dosimetry can produce discrepancies of as much as −74% to 62% in individual patients for red marrow self-dose due to ^{124}I-labeled antibodies, in comparison with PET image–based dosimetry. Projected differences for other radionuclides between plasma- and appropriate image-based dose estimates would depend on additional factors, including physical half-life and photon yield, but are likely to be of the same order. The implication is that individualized imaged-based dosimetry would be optimal for therapeutic delivery of radiolabeled antibodies, both in terms of maximizing radiation dose to target tissues and in terms of remaining within the tolerance of red marrow. Of course, PET may not always be appropriate, either because of the lack of applicable positron-emitting radionuclides or for other reasons, including cost. However, continual improvements in quantitative SPECT may enable a SPECT image–based approach to be adopted. In this study, we examined the use of a hybrid dosimetry scheme combining both image- and plasma-based data and found it to be a closer approximation to an exclusively image-based approach. A clinically practicable scheme could include an initial image-based assessment of RMPR(0) together with a standardized value of effective marrow accumulation rate coupled with regular blood or plasma measurements. This would require initial pilot studies to more fully characterize the kinetics of antibody accumulation in bone marrow.

The work presented here is limited by several factors, most significantly the small number of patients and imaging time-points. Further work is required to corroborate the results and fully characterize the mechanisms involved. At a more immediate level, it was assumed for dosimetric purposes that the image-derived activity concentration within the marrow spaces was uniform and equal to the red marrow activity concentration. However, some of this space may be composed of adipose tissue (i.e., yellow marrow) with reduced activity concentration. It has been proposed that marrow cellularity may be defined as approximately equal to 1 − (fat fraction), that is, the fraction of the marrow space that is not taken up by fat cells (31,32). Shah et al. (33) developed an image-based transport model for skeletal dosimetry (and lumbar vertebrae in particular) in which they determined that, for the electron energies of interest in this study, assuming that the marrow cellularity is 100% yields results that have an approximately 13%–20% error compared with those obtained by including a realistic adipocyte fraction. However, the adipocyte fraction is dependent on the age and health of the patient and is highly variable even among healthy patients. If values of adipocyte fraction were available for individual patients, red marrow activity concentrations could be scaled upward accordingly. Irrespective of this issue, the general trends and implications discussed in this paper would not be significantly affected.

CONCLUSION

Red marrow self-dose was estimated by ROI analysis of ^{124}I-labeled antibody PET images and compared with estimates based on plasma activity concentration measurements. Values of RMPR were dependent on patient-specific factors and were observed to increase over the 7-d timescale of the study for both ^{124}I-cG250 and ^{124}I-huA33. The data suggest that individualized imaged-based dosimetry is required for optimal therapeutic delivery of radiolabeled antibodies.

DISCLOSURE STATEMENT

ACKNOWLEDGMENTS

REFERENCES

1. Siegel JA, Pawlyk DA, Lee RE, et al. Tumor, red marrow, and organ dosimetry for ^{131}I-labeled anti-carcinoembryonic antigen monoclonal antibody. *Cancer Res.* 1990;50:1039s–1042s.

2. Thomas SR, Maxon HR, Kereiakes JG, Saenger EL. Quantitative external counting techniques enabling improved diagnostic and therapeutic decisions in patients with well-differentiated thyroid cancer. *Radiology.* 1977;122:731–737.

3. King M, Farncombe T. An overview of attenuation and scatter correction of planar and SPECT data for dosimetry studies. *Cancer Biother Radiopharm.* 2003;18:181–190.

4. DeNardo GL, Siantar CL, DeNardo SJ. Radiation dosimetry for radionuclide therapy in a nonmyeloablative strategy. *Cancer Biother Radiopharm.* 2002;17:107–118.

5. Buchegger F, Chalandon Y, Pelegrin A, Hardman N, Mach JP. Bone marrow dosimetry in rats using direct tissue counting after injection of radio-iodinated intact monoclonal antibodies or F(ab′)2 fragments. *J Nucl Med.* 1991;32:1414–1421.

6. Johnson TK, Gonzalez R, Kasliwal RK, et al. Distribution of a breast-directed I-131-radiolabeled monoclonal antibody in blood and bone marrow: implications for radiation immunotherapy. *Radiology.* 1992;182:107–114.

7. Sgouros G. Bone marrow dosimetry for radioimmunotherapy: theoretical considerations. *J Nucl Med.* 1993;34:689–694.

8. Siegel J, Wessels B, Watson E, et al. Bone marrow dosimetry and toxicity for radioimmunotherapy. *Antibody Immunoconjugates Radiopharm.* 1990;3:213–234.

9. Sgouros G, Stabin M, Erdi Y, et al. Red marrow dosimetry for radiolabeled antibodies that bind to marrow, bone, or blood components. *Med Phys.* 2000;27:2150–2164.

10. Wessels BW, Bolch WE, Bouchet LG, et al. Bone marrow dosimetry using blood-based models for radiolabeled antibody therapy: a multiinstitutional comparison. *J Nucl Med.* 2004;45:1725–1733.

11. Williams LE, DeNardo GL, Meredith RF. Targeted radionuclide therapy. *Med Phys.* 2008;35:3062–3068.

12. Wiseman GA, White CA, Stabin M, et al. Phase I/II ^{90}Y-Zevalin (yttrium-90 ibritumomab tiuxetan, IDEC-Y2B8) radioimmunotherapy dosimetry results in relapsed or refractory non-Hodgkin's lymphoma. *Eur J Nucl Med.* 2000;27:766–777.

13. Phelps ME. PET: the merging of biology and imaging into molecular imaging. *J Nucl Med.* 2000;41:661–681.

14. Phelps ME. Positron emission tomography provides molecular imaging of biological processes. *Proc Natl Acad Sci USA.* 2000;97:9226–9233.

15. Divgi CR, Pandit-Taskar N, Jungbluth AA, et al. Preoperative characterisation of clear-cell renal carcinoma using iodine-124-labelled antibody chimeric G250 ([124]I-cG250) and PET in patients with renal masses: a phase I trial. *Lancet Oncol.* 2007;8:304–310.

16. Carrasquillo JA, Pandit-Taskar N, O'Donoghue JA, et al. [124]I-huA33 antibody PET of colorectal cancer. *J Nucl Med.* 2011;52:1173–1180.

17. Lubberink M, Herzog H. Quantitative imaging of [124]I and [86]Y with PET. *Eur J Nucl Med Mol Imaging.* 2011;38(suppl 1):S10–S18.

18. Pentlow KS, Graham MC, Lambrecht RM, et al. Quantitative imaging of iodine-124 with PET. *J Nucl Med.* 1996;37:1557–1562.

19. Pentlow KS, Graham MC, Lambrecht RM, Cheung NK, Larson SM. Quantitative imaging of I-124 using positron emission tomography with applications to radioimmunodiagnosis and radioimmunotherapy. *Med Phys.* 1991;18:357–366.

20. Pryma DA, O'Donoghue JA, Humm JL, et al. Correlation of in vivo and in vitro measures of carbonic anhydrase IX antigen expression in renal masses using antibody [124]I-cG250. *J Nucl Med.* 2011;52:535–540.

21. O'Donoghue JA, Smith-Jones PM, Humm JL, et al. [124]I-huA33 antibody uptake is driven by A33 antigen concentration in tissues from colorectal cancer patients imaged by immuno-PET. *J Nucl Med.* 2011;52:1878–1885.

22. Mageras GA, McNamara S, Pham H, Xiong JP. Imaging for radiation treatment planning. In: Starkschall BCG, ed. *Informatics in Radiation Oncology.* Baton Rouge, LA: CRC Press. In press.

23. Humm JL, Lee J, O'Donoghue JA, et al. Changes in FDG tumor uptake during and after fractionated radiation therapy in a rodent tumor xenograft. *Clin Positron Imaging.* 1999;2:289–296.

24. Beddoe AH, Darley PJ, Spiers FW. Measurements of trabecular bone structure in man. *Phys Med Biol.* 1976;21:589–607.

25. Hough M, Johnson P, Rajon D, Jokisch D, Lee C, Bolch W. An image-based skeletal dosimetry model for the ICRP reference adult male: internal electron sources. *Phys Med Biol.* 2011;56:2309–2346.

26. Stabin MG, Sparks RB, Crowe E. OLINDA/EXM: the second-generation personal computer software for internal dose assessment in nuclear medicine. *J Nucl Med.* 2005;46:1023–1027.

27. Hindorf C, Linden O, Tennvall J, Wingardh K, Strand SE. Time dependence of the activity concentration ratio of red marrow to blood and implications for red marrow dosimetry. *Cancer.* 2002;94:1235–1239.

28. Oosterwijk E, Bander NH, Divgi CR, et al. Antibody localization in human renal-cell carcinoma: a phase-I study of monoclonal antibody-G250. *J Clin Oncol.* 1993;11:738–750.

29. Welt S, Ritter G, Williams C, et al. Phase I study of anticolon cancer humanized antibody A33. *Clin Cancer Res.* 2003;9:1338–1346.

30. Garinchesa P, Sakamoto J, Welt S, Real FX, Rettig WJ, Old LJ. Organ-specific expression of the colon cancer antigen A33, a cell surface target for antibody-based therapy. *Int J Oncol.* 1996;9:465–471.

31. Bolch WE, Patton PW, Rajon DA, Shah AP, Jokisch DW, Inglis BA. Considerations of marrow cellularity in 3-dimensional dosimetric models of the trabecular skeleton. *J Nucl Med.* 2002;43:97–108.

32. Jokisch DW, Rajon DA, Patton PW, Bolch WE. Methods for the inclusion of shallow marrow and adipose tissue in pathlength-based skeletal dosimetry. *Phys Med Biol.* 2011;56:2699–2713.

33. Shah AP, Bolch WE, Rajon DA, Patton PW, Jokisch DW. A paired-image radiation transport model for skeletal dosimetry. *J Nucl Med.* 2005;46:344–353.